*Inorg. Chem.* **2008**, *47*, 11095−11107

# Role of Inner- and Outer-Sphere Bonding in the Sensitization of $Eu^{III}$-Luminescence Deciphered by Combined Analysis of Experimental Electron Density Distribution Function and Photophysical Data

**Lada N. Puntus,*,† Konstantin A. Lyssenko,‡ Mikhail Yu. Antipin,‡ and Jean-Claude G. Bünzli§**

*Laboratory of Molecular Nanoelectronics, Institute of Radio Engineering & Electronics, Russian Academy of Sciences, 11-7 Mokhovaya, Moscow, 125009, Russia, A. N. Nesmeyanov Institute of Organoelement Compounds, Russian Academy of Sciences, GSP-1, 28 Vavilov Street, Moscow, 119991, Russia, and Laboratory of Lanthanide Supramolecular Chemistry, Swiss Federal Institute of Technology Lausanne (EPFL), CH-1015 Lausanne, Switzerland*

Received July 25, 2008

A series of lanthanide adducts with different amounts of 1,10-phenanthroline, chloride ions, and water molecules in the inner and outer coordination spheres are investigated with the aim of relating the chemical bonding pattern in the crystals to the luminescence properties of the Eu ion: $[LnCl_1Phen_2(H_2O)_3]Cl_2(H_2O)$ (Ln = Eu, **1Eu**; Gd, **1Gd**; Tb, **1Tb**), $[EuCl_2Phen_2(H_2O)_2]Cl_1(H_2O)$ (**2**), and $[EuCl_2Phen_1(H_2O)_4]Cl_1(H_2O)$ (**3**). The influence of inner- versus outer-sphere ligands on the Ln−X bond lengths and angles in the structure is examined. A detailed topological analysis of the electron density function derived from the X-ray diffraction data for **1Gd** is performed within the frame of the "atoms in molecule" theory for the first time for a lanthanide complex. The chemical bonding pattern is interpreted in terms of net atomic charges, bond energies, and electron transfers from the ligands to the metal ion. A noteworthy finding is that the energy of extended noncovalent interactions occurring in the second coordination sphere (H-bonding and $\pi$-stacking interactions) is comparable to that of Ln−ligand bonds. The luminescence properties of the three Eu adducts are interpreted with the results of electron density distribution function topology. An intraligand charge transfer state is identified, and its contribution in the ligand-to-europium energy transfer process is analyzed. The outcome of this study is that specific interionic interactions which are usually not considered in theoretical calculations or in the interpretation of luminescence properties play an important role in the sensitization of the Eu luminescence.

## 1. Introduction

The ever growing interest in lanthanide molecular complexes and materials with optical properties stems from applications in multidisciplinary fields such as nanosensors,[1a] materials for telecommunications,[1b] lighting devices,[1c] and luminescent probes for bioanalyses and live cell imaging and sensing.[1e] Most of these applications use the unique ability of the lanthanides to emit well-defined narrow bands in different spectral ranges, from visible to near-infrared. Due to the low absorption cross-section of the f−f transitions, efficient population of the excited f states has to rely on energy transfer from the surroundings of the metal ion (antenna effect or luminescence sensitization).[2] The latter phenomenon is rather complex, involving several electronic states from both the ligands and the metal ion, as well as

* Author to whom correspondence should be addressed. E-mail: lada_puntus@mail.ru.

† Institute of Radio Engineering & Electronics, Russian Academy of Sciences.

‡ A. N. Nesmeyanov Institute of Organoelement Compounds, Russian Academy of Sciences.

§ Swiss Federal Institute of Technology Lausanne.

(1) (a) Martin, L. J.; Hahnke, M. J.; Nitz, M.; Wohnert, J.; Silvaggi, N. R.; Allen, K. N.; Schwalbe, H.; Imperiali, B. *J. Am. Chem. Soc.* **2007**, *129*, 7106–7113. (b) Kido, J; Okamoto, Y. *Chem. Rev.* **2002**, *102*, 2357–2368. (c) Shionoya, S.; Yen, W. M. *Phosphor Handbook*; CRC Press Inc.: Boca Raton, 1999. (d) Ozawa, L.; Itoh, M. *Chem. Rev.* **2003**, *103*, 3835–3856. (e) Matsumoto, K.; Yuan, J. G. *Lanthanide Chelates as Fluorescent Labels for Diagnostics and Biorechnology, Metal Ions in Biological Systems*; Sigel, A., Sigel, H., Eds.; Marcel Dekker Inc.: New York, 2003; Vol. *40*, Chapter 6. (f) Bunzli, J.-C. G. *Metal Complexes in Tumor Diagnosis and as Anticancer Agents* Sigel, A., Sigel, H., Eds.; Marcel Dekker Inc.: New York, 2004, vol. 42, Chapter 2, p. 39.

(2) Bünzli, J.-C.G.; Piguet, C. *Chem. Soc. Rev.* **2005**, *34*, 1048–1077.

10.1021/ic801402u CCC: $40.75 
Published on Web 10/25/2008

several different mechanisms.[3] As a consequence and despite the progress made during the past few decades in both the understanding and the modeling of ligand-to-metal energy transfers, the design of highly luminescent lanthanide tags still relies on trial and error procedures. The final photophysical properties are indeed very dependent on very small variations (~0.01Å) of the donor-metal bond lengths and of the chromophore spatial orientation. This is also true when quenching through ligand-to-metal charge transfer (LMCT) states and vibrations occur, the geometrical parameters being again very critical.

A deeper understanding of the chemical binding in luminescent lanthanide tags is therefore needed, with respect to both innersphere binding and noncovalent second-sphere interactions. One way to address this problem is to turn to a combination of accurate X-ray diffraction data with *ab initio* calculations and spectroscopic data. To date, available *ab initio* calculations for lanthanide compounds still vary widely in their predictions and estimated bond lengths; energies and atomic charges heavily depend on the level of theory, a functional in the case of DFT calculations and a pseudopotential basis set.[4] For instance, despite the fact that the present accuracy of bond lengths determined by X-ray diffraction attains on average ±0.005Å, an accuracy lower by a factor 2 is often considered as being acceptable for quantum chemical calculation.[5,6] Finally, description of the chemical bonding pattern in lanthanide complexes remains controversial with respect to the involvement of f orbitals, particularly when it comes to estimating the covalent contribution,[7] the role of direct and back-donation,[5] the influence of coordinated and noncoordinated counterions, and interionic or intermolecular interactions[5,6,8] linked to the supramolecular organization of the crystal structure.

In order to deepen the understanding of these phenomena and to decipher quantitative relationships between luminescent properties and the complex formulation, geometry, and bonding pattern, a set of lanthanide adducts containing different amounts of 1,10-phenanthroline (phen) as well as inner- and outer-sphere chloride ions and water molecules has been analyzed in detail. Despite the fact that these complexes have been known for a long time,[9] no precise structural information is available and no high-level theoretical calculations have been carried out. In this paper, we therefore investigate the chemical bonding pattern for these systems on the basis of the electron density function from high-resolution X-ray diffraction data. The topological analysis of the electron density function also allows one to estimate the energies of intra- and interatomic interactions in the crystals.[10] The accuracy of this approach is well-documented for light elements, but data are much scarcer for heavy transition elements such as the lanthanides.[11] The consequences of the chemical bond mapping extracted from these data on the energy transfer processes leading to $Eu^{III}$ sensitized emission are presented. The role of the various factors mentioned above is elucidated, and a new sensitizing pathway is unraveled.

## 2. Experimental Section

**Complexes.** The following complexes of lanthanide chlorides with phen were synthesized according to slightly modified published procedures:[12,13] $[LnCl_1Phen_2(H_2O)_3]Cl_2(H_2O)$, with Ln = Eu (**1Eu**), Gd (**1Gd**), and Tb (**1Tb**); $[EuCl_2Phen_2(H_2O)_2]Cl_1(H_2O)$ (**2**); and $[EuCl_2Phen_1(H_2O)_4]Cl_1(H_2O)$ (**3**). For obtaining complexes **1**, 3−4 drops of bidistillated water were added to the final solution.

**Complexes 1Eu and 2.** Yield 97%. Anal. calcd for $C_{24}H_{22}N_4O_3EuCl_3$ (672.8): C, 42.85%; H, 3.30%; N, 8.33%. Found: C, 42.22%; H, 3.22%; N, 8.25%.

**Complex 3.** Yield 92%. Anal. calcd for $C_{12}H_{18}N_2O_5EuCl_3$ (528.6): C, 27.27%; H, 3.43%; N, 5.29%. Found: C, 27.18%; H, 3.26%; N, 5.16%.

**$TbCl_3Phen_2(H_2O)_3$.** Yield 95%. Anal. calcd for $C_{24}H_{22}N_4O_3TbCl_3$ (679.8): C, 42.41%; H, 3.26%; N, 8.24%. Found: C, 42.02%; H, 3.20%; N, 8.18%.

**$GdCl_3Phen_2(H_2O)_3$.** Yield 90%. Anal. calcd for $C_{24}H_{22}N_4O_3GdCl_3$ (678.1): C, 42.51%; H, 3.27%; N, 8.26%. Found: C, 42.32%; H, 3.22%; N, 8.19%.

Single crystals of all complexes were grown by slow evaporation from ethanol solutions over 2−3 days.

**X-Ray Crystallography.** All diffraction data were taken using a Bruker SMART APEX II CCD diffractometer [$\lambda$(Mo K$\alpha$) = 0.71072Å, $\omega$-scans] (see Table 1). Substantial redundancy in data allowed empirical absorption corrections to be applied with the SADABS program[14] using multiple measurements of equivalent reflections. The structures were solved by the direct method and refined by the full-matrix least-squares technique with respect to $F^2$ in the anisotropic−isotropic approximation. The hydrogen atoms of water molecules were located from the difference Fourier density synthesis and refined within the riding model. All calculations were performed using the SHELXTL software.[15]

The multipole refinement of **1Gd** was carried out within Hansen−Coppens' formalism[16] with the XD program package[17]


(3) De Sá, G. F.; Malto, O. L.; Donega, C. D.; Simas, A. M.; Longo, R. L.; Sant-Cruz, P. A.; da Silva, E. F. *Coord. Chem. Rev.* **2000**, *196*, 165–195.
(4) Clark, A. E. *J. Chem. Theory Comput.* **2008**, *4*, 708–718.
(5) Guillaumont, D. *J. Phys. Chem. A* **2004**, *108*, 6893–6900.
(6) Guillaumont, D. *THEOCHEM* **2006**, *771*, 105–110.
(7) (a) Perrin, L.; Maron, L.; Eisenstein, O. *Faraday, Discuss.* **2003**, *124*, 25–39. (b) Eisenstein, O.; Maron, L. L. *J. Organomet. Chem.* **2002**, *647*, 190–197. (c) Villa, A.; Cosentino, U.; Pitea, D.; Moro, G.; Maiocchi, A. *J. Chem. Phys. A* **2000**, *104*, 3421–3429. (d) Schinzel, S.; Bindl, M.; Visseaux, M.; Chermette, H. *J. Phys. Chem. A* **2006**, *110*, 11324–11331. (e) Clark, D. L.; Gordon, J. C.; Hay, P. J.; Poli, R. *Organometallics* **2005**, *24*, 5747–5758. (f) Clavague'ra, C.; Dognon, J.-P.; Pyykkö, P. *Chem. Phys. Lett.* **2006**, *429*, 8–12.
(8) Bombiere, G. N.; Marchini, N; Ciattini, S.; Mortillaro, A.; Aime, S. *Inorg. Chim. Acta* **2006**, *359*, 3405–3411.
(9) Liu, W. S.; Tan, M. Y. *Thermochim. Acta* **1991**, *191*, 135–142.
(10) (a) Koritsanszky, T. S.; Coppens, P. *Chem. Rev.* **2001**, *101*, 1583. (b) Gatti, C. *Z. Kristallogr.* **2005**, *220*, 399. (c) Tsirelson, V. G.; Ozerov, R. P. *Electron Density and Bonding in Crystals: Principles, Theory and X-Ray Diffraction Experiments in Solid State Physics and Chemistry*; IOP Publishing Ltd.: Philadelphia, PA, 1996. (d) Matta, C.; Boyd, R. J. *The Quantum Theory of Atoms in Molecules*; Wiley-VCH: Weinheim, Germany, 2007.
(11) Coppens, P.; Iversen, B.; Larsen, F. K. *Coord. Chem. Rev.* **2005**, *249*, 179–195.
(12) Hart, F. A.; Laming, F. P. *J. Inorg. Nucl. Chem.* **1964**, *26*, 579–591.
(13) Puntus, L.; Lyssenko, K. *J. Rare Earths* **2008**, *26*, 146–152.
(14) *SADABS*, version 2004/1; Bruker AXS Inc.: Madison, WI. *XPREP*, version 2005/2; Bruker AXS Inc.: Madison, WI.
(15) *SHELXTL*, version 6.1; Bruker AXS Inc.: Madison, WI, 2005.
(16) Hansen, N. K.; Coppens, P. *Acta Crystallogr., Sect. A* **1978**, *34*, 909–921.
(17) Volkov, A.; Macchi, P.; Farrugia, L. J.; Gatti, C.; Mallinson, P.; Richter, T.; Koritsanszky, T. *XD2006*; SUNY at Buffalo: Buffalo, NY, 2006.

**Table 1.** Crystal Data and Structure Refinement Parameters for **1**−**3**[a]

| compound | **1Eu** | **1Gd**[a] | **1Tb** | **2** | **3** |
|---|---|---|---|---|---|
| formula | $C_{24}H_{24}Cl_3EuN_4O_4$ | $C_{24}H_{24}Cl_3GdN_4O_4$ | $C_{24}H_{24}Cl_3TbN_4O_4$ | $C_{24}H_{22}Cl_3EuN_4O_3$ | $C_{12}H_{18}Cl_3EuN_2O_5$ |
| fw | 690.78 | 696.07 | 697.74 | 672.77 | 528.59 |
| $T$ | 100 | 100 | 100 | 100 | 120 |
| cryst syst | triclinic | triclinic | triclinic | orthorhombic | triclinic |
| space group | $P\bar{1}$ | $P\bar{1}$ | $P\bar{1}$ | $Pca2_1$ | $P\bar{1}$ |
| $a$ (Å) | 10.3407(4) | 10.3337(2) | 10.3057(6) | 36.2101(6) | 7.8874(14) |
| $b$ (Å) | 10.4846(4) | 10.4819(2) | 10.4724(8) | 7.6163(1) | 9.2112(17) |
| $c$ (Å) | 12.5381(5) | 12.5371(2) | 12.5438(9) | 18.0859(3) | 13.268(2) |
| α (deg) | 97.4427(8) | 97.5218(7) | 97.568(3) | | 106.734(4) |
| $\beta$ (deg) | 108.4136(7) | 108.4846(6) | 108.542(3) | | 97.205(4) |
| $\gamma$ (deg) | 93.4485(8) | 93.4024(7) | 93.415(2) | | 105.200(4) |
| $V$ (Å$^3$) | 1271.49(9) | 1269.47(4) | 1264.90(15) | 4987.86(13) | 869.5(3) |
| $Z(Z')$ | 2(1) | 2(1) | 2(1) | 8(2) | 2(1) |
| $F$(000) | 684 | 686 | 688 | 2656 | 516 |
| $D_{calcd}$ (g cm$^{-1}$) | 1.804 | 1.821 | 1.832 | 1.792 | 2.091 |
| $\mu$ (cm$^{-1}$) | 28.21 | 29.67 | 31.52 | 28.71 | 40.91 |
| $\theta$ range (deg) | 1.73−30.0 | 1.73−30.0 | 1.73−29.0 | 1.59−31.00 | 3−27.0 |
| reflns measured | 12723 | 86623 | 14254 | 66948 | 7845 |
| independent reflns [$R_{int}$] | 7243 [0.0194] | 7382 [0.0258] | 6680 [0.0282] | 15872 [0.0532] | 3960 [0.0820] |
| obsd reflns [$I > 2\sigma(I)$] | 6606 | 7194 | 5982 | 14122 | 2345 |
| final $R(F_{hkl})$: $R_1$ | 0.0237 | 0.0123 | 0.0252 | 0.0308 | 0.0468 |
| $wR_2$ | 0.0509 | 0.0317 | 0.0546 | 0.0627 | 0.0943 |
| GOF | 1.004 | 1.080 | 0.983 | 1.016 | 0.639 |
| $\Delta\rho_{max}$, $\Delta\rho_{min}$ ($e$ Å$^{-3}$) | 0.866/−0.802 | 0.817/−0.412 | 0.907/−0.751 | 0.990 /−1.408 | 1.601/−1.858 |

[a] For multipole refinement of **1Gd**, the high-resolution data (249 108 measured reflection with $2\theta_{max} < 110°$; 31 917 independent reflections, $R_{int} = 0.0348$, $wR_2 = 0.0444$, GOF = 0.968, $R_1 = 0.0202$ (28 672 observed reflections with $I > 2\sigma(I)$) was used.

and scattering factors determined from STO atomic relativistic wave functions at the PBE/QZ4P level.[18] The refinement was carried out with respect to $F$ and converged to $R = 0.0146$, $Rw = 0.0127$, and GOF = 0.8389 for 26 721 merged reflections with $I > 3\sigma(I)$ and $F_{obs} > 6$. All C−C and N−C bonded pairs of atoms satisfy the Hirshfeld rigid-bond criteria (the maximum difference of the mean-square displacement amplitudes was $9 \times 10^{-4}$ Å$^2$). For Gd−O, the corresponding values were slightly larger but did not exceed $15 \times 10^{-4}$ Å$^2$. The residual electron density for reflections with $2\theta < 75°$ was smaller than 0.31 $e$ Å$^{-3}$. Topological analysis of the experimental $\rho(\mathbf{r})$ function was carried out using the *WinXPRO* program package.[19]

The kinetic energy $[g(\mathbf{r})]$ was estimated from experimental diffraction data within the frame of Kirzhnits's approximation,[20] which relates it to values of $\rho(\mathbf{r})$ and its derivatives: $g(\mathbf{r}) = (3/10)(3\pi^2)^{2/3}[\rho(\mathbf{r})]^{5/3} + (1/72)|\nabla\rho(\mathbf{r})|^2/\rho(\mathbf{r}) + 1/6\nabla^2\rho(\mathbf{r})$. Use of this relationship in conjunction with the virial theorem $[2g(\mathbf{r}) + v(\mathbf{r}) = 1/4\nabla^2\rho(\mathbf{r})]$ provided values of the potential energy density $v(\mathbf{r})$ at the critical points. Moreover, this method allows one to estimate the atomic energy by integration of the electron energy density function $h_e(\mathbf{r}) = g(\mathbf{r}) + v(\mathbf{r})$ over the atomic basin. The accuracy of this approach for closed-shell and intermediate types of interatomic interactions was shown for various complexes (see, for example, ref 21).

**Physico-Chemical Measurements.** Low-resolution luminescence measurements (spectra and lifetimes) were recorded on a Fluorolog FL 3-22 spectrometer from Horiba-Jobin-Yvon-Spex at 293 and 77 K. Phosphorescence lifetimes ($\tau$) were measured using a quartz capillary; they are averages of at least three independent measurements, which were made by monitoring the decay at the maxima of the emission spectra, enforcing a 0.05 ms delay. The decays, single or biexponential, were analyzed with Origin 7.0. Absolute quantum yields ($Q$) of europium-centered luminescence were determined by an absolute method[22] with a specially designed integration sphere.[23] High-resolution laser-excited luminescence spectra and lifetimes have been measured at variable temperatures using published procedures.[24] Reflectance IR spectra were obtained from powdered samples with a Perkin-Elmer Spectrum One FT-IR spectrometer.

## 3. Results and Discussion

**3.1. Molecular Geometry and Crystal Structures.** According to X-ray diffraction data, the metal atoms are eight-coordinated in all of the isolated complexes (Figure 1, Table 2). In the isostructural complexes **1Eu**, **1Gd**, and **1Tb**, the metal ion is coordinated to one chloride anion, while two chlorides are bound in the inner coordination sphere of complexes **2** and **3**. There are two coordinated phens in **1** and **2** and one coordinated phen in complex **3**. Henceforth, the available experimental data lend themselves to the analysis of the change in the metal−phen bonding as a function of the number of innersphere counterions. The role of crystal packing effects could also be analyzed by comparison of two symmetry-independent cations in the crystal of **2**, designated as **2A** and **2B**.

There are three idealized polyhedra for eight-coordination, trigonal dodecahedron ($D_{2d}$), bicapped trigonal prism ($C_{2v}$), and square antiprism ($D_{4d}$), which can be assigned with the help of the so-called shape measure parameter

(18) Volkov, A.; Macchi, P. unpublished work
(19) (a) Stash, A.; Tsirelson, V. *WinXPRO*; Mendeleev University of Chemical Technology: Moscow, Russia, 2001. (b) Stash, A.; Tsirelson, V. G. *J. Appl. Crystallogr.* **2002**, *35*, 371–373.
(20) Bader, R. F. W. *J. Phys. Chem. A* **1998**, *102*, 7314–7323.
(21) (a) Tsirelson, V. G. *Acta Crystallogr., Sect. B* **2002**, *58*, 632–639. (b) Farrugia, L. J.; Cameron, E. *J. Phys. Chem. A* **2005**, *109*, 8834–8848.
(22) De Mello, J. C.; Wittmann, H. C.; Friend, R. H. *Adv. Mater.* **1997**, *9*, 230–235.
(23) Gumy, F. Patent application PCT/IB2007/054187, 15.10.2007.
(24) Rodriguez-Cortinas, R.; Avecilla, F.; Platas-Iglesias, C.; Imbert, D.; Bünzli, J.-C. G.; de Blas, A.; Rodriguez-Blas, T. *Inorg. Chem.* **2002**, *41*, 5336–5349.

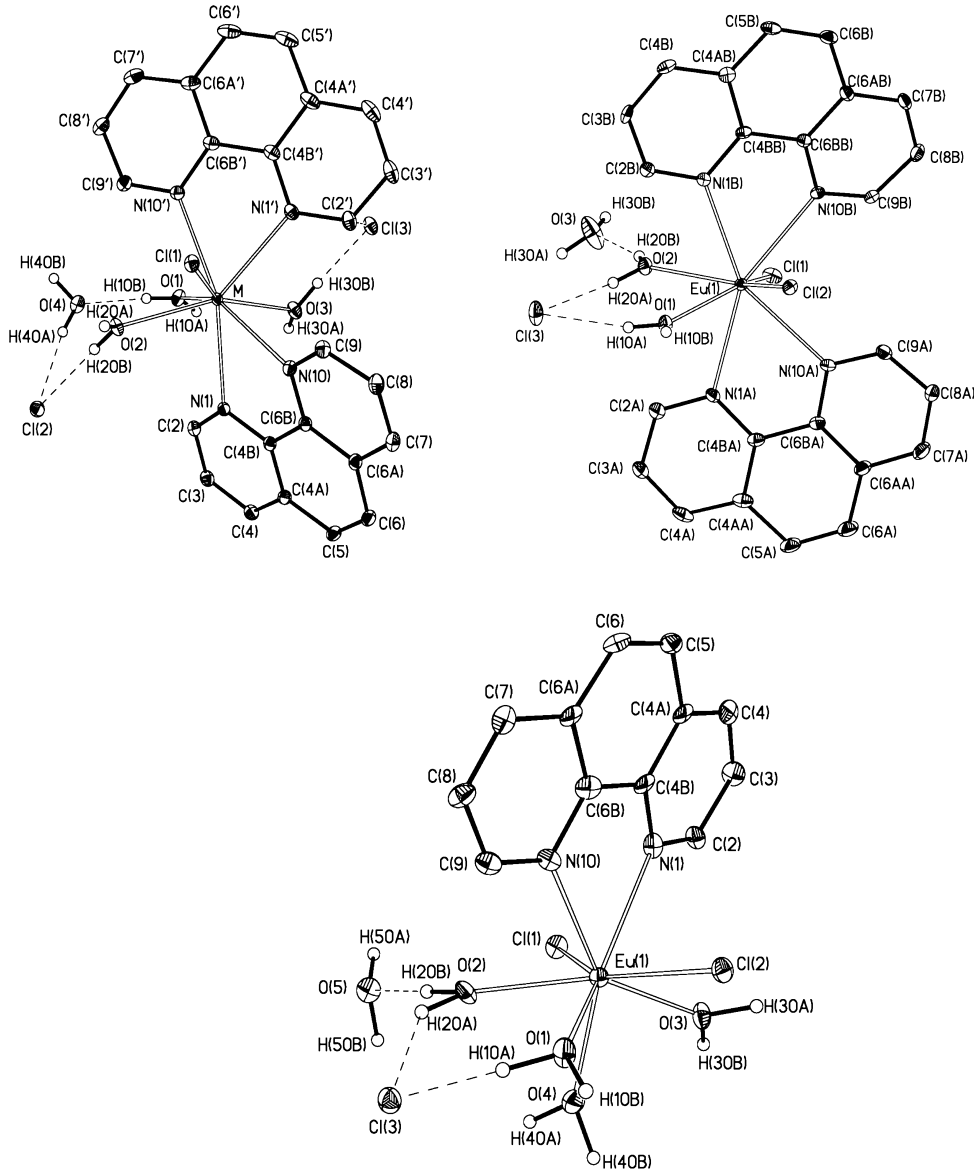


**Figure 1.** General view of structures **1**−**3** with thermal ellipsoids set at the 50% probability.

**Table 2.** Selected Bond Lengths (Å) in Europium Complexes **1**−**3**

| | | **2** | | | | | |
|---|---|---|---|---|---|---|---|
| **1Eu** | | **2A** | | **2B** | | **3** | |
| Eu(1)−Cl(1) | 2.7103(5) | Eu(1)−Cl(1) | 2.7051(8) | Eu(1′)−Cl(1′) | 2.6796(9) | Eu(1)−Cl(1) | 2.7483(19) |
| Eu(1)−O(1) | 2.3882(16) | Eu(1)−Cl(2) | 2.7002(8) | Eu(1′)−Cl(2′) | 2.7006(8) | Eu(1)−Cl(2) | 2.749(2) |
| Eu(1)−O(2) | 2.3899(15) | Eu(1)−O(1) | 2.398(2) | Eu(1′)−O(1′) | 2.410(3) | Eu(1)−O(1) | 2.397(5) |
| Eu(1)−O(3) | 2.4216(15) | Eu(1)−O(2) | 2.406(2) | Eu(1′)−O(2′) | 2.417(3) | Eu(1)−O(2) | 2.420(5) |
| Eu(1)−N(1) | 2.5794(19) | Eu(1)−N(1A) | 2.614(3) | Eu(1′)−N(1C) | 2.585(3) | Eu(1)−O(4) | 2.422(6) |
| Eu(1)−N(10) | 2.5539(18) | Eu(1)−N(10A) | 2.606(3) | Eu(1′)−N(10C) | 2.630(3) | Eu(1)−O(3) | 2.369(5) |
| Eu(1)−N(1′) | 2.5688(19) | Eu(1)−N(1B) | 2.580(3) | Eu(1′)−N(1D) | 2.630(3) | Eu(1)−N(1) | 2.565(7) |
| Eu(1)−N(10′) | 2.5630(18) | Eu(1)−N(10B) | 2.604(3) | Eu(1′)−N(10D) | 2.624(3) | Eu(1)−N(10) | 2.574(7) |
| | | | Mean Bond Lengths | | | | |
| Eu−Cl | 2.7103 | | 2.7026 | | 2.690 | | 2.7486 |
| Eu−O | 2.400 | | 2.402 | | 2.413 | | 2.402 |
| Eu−N | 2.566 | | 2.601 | | 2.617 | | 2.570 |

(*S*) calculated from dihedral angles along all edges.[25] The latter points to the square antiprism being the best description of the coordination polyhedra in structures **1**−**3**. The ligands arrange themselves in such a way as to minimize both electrostatic repulsions and steric hindrance; the chloride anions are localized above the phen ligands (Scheme 1). The mean square displacement of atoms from the base plane, the dihedral angles between the two base squares, and the distance between the metal ion and the polyhedron center allow one to estimate the

(25) Xu, J.; Radkov, E.; Ziegler, M.; Raymond, K. N. *Inorg. Chem.* **2000**, *39*, 4156–4164.

**Scheme 1.** Schematic Representation of Square Antiprism Polyhedra in the Europium Complexes **1Eu**, **2**, and **3** in Newman Projection[a]

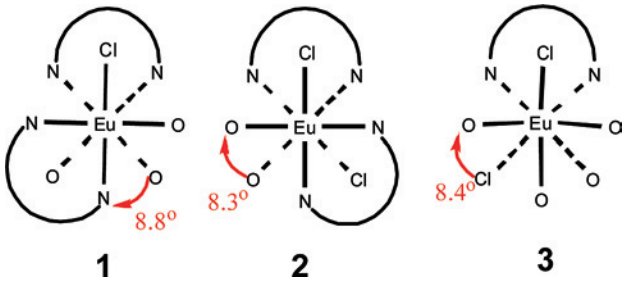


[a] Bonds to donor atoms forming the bottom plane are drawn with dashed lines; arrows indicate angle between base planes.

degree of distortion with respect to the idealized geometry (Table S1, Supporting Information). Judging from these data, variation in the number of chloride anions and phen ligands does not affect significantly the polyhedron distortion, while the latter is more sensitive to the crystal packing (compare the two independent molecules **2A** and **2B**). An interesting feature is the decreasing dihedral angle between phen ligands when the number of coordinated chloride anions increases. This tendency has also been observed for the $[Eu(phen)_2(H_2O)_5]Cl_3$[13] complex, in which the phen ligands are almost perpendicular to each other. Such dependence is especially important in view of supramolecular organization because the perpendicular orientation of phen ligands facilitates additional stacking interactions in the crystals.

In contrast to polyhedron distortion, the bond length distribution is more sensitive to the nature of the ligands, as demonstrated with the europium complexes. The average Eu−N, Eu−O, and Eu−Cl bond lengths are listed in Table 2, and the following trends are observed: (i) the Eu−Cl bond length is the most sensitive to the composition of the coordination sphere, for example, ca. 2.75 Å in **3** compared to ca. 2.70 Å in **1Eu** and **2**; (ii) the mean Eu−N distance is the same in **1Eu** and **3** but longer by 0.04 Å in **2**; (iii) the mean Eu−O distance remains fairly the same in all three complexes.

The different ratios of coordinated to noncoordinated water molecules and chloride anions lead to different intermolecular interactions and henceforth to different supramolecular assemblies, H-bonded layers in **1Eu**, double chains in **2**, and double layers in **3**; the latter H-bonded aggregates are assembled into 3D frameworks by stacking interactions. The crystal packing of the complexes is determined by the number of noncovalent interactions such as H bonds (O−H···O, O−H···Cl, C−H···Cl, C−H···O, and C−H···$\pi$), stacking interactions (C···C and C···N), and even Cl···$\pi$ contacts. From the energetic point of view, one can expect that stacking and especially H bonds play a major role. The O−H···Cl interactions in all complexes can be considered as rather strong with interatomic O···Cl distances varying in the range 3.026(2)−3.219(2) Å (see Tables S2−S4, Supporting Information). The strength of the O−H···O interactions depends on the complex and varies from moderate in **1Eu** and **2** (with O···O contacts in the range 2.635(4)−2.656(4) Å) to weak in **3** (2.794(4)−2.834(4) Å). These H bonds affect metal−ligand bonds, causing either an elongation of the Ln−Cl bonds or a shortening of the M−$OH_2$ ones upon increasing the strength of H bonding. A similar correlation has been reported for Ln−O bonds in the isostructural complexes $[Ln(H_2O)_9](SO_3CF_3)_3$.[26] In crystals of **1Eu**, **2**, and **3**, however, it is more difficult to correlate the coordination geometry with the peculiarities of the crystal packing due to competing factors, as can be illustrated for **2**. In this compound, the two independent molecules **2A** and **2B** have the same mutual disposition of ligands (Scheme 1), but differences of ca. 0.02 and 0.04 Å are observed for Eu−Cl, Eu−O, and Eu−N bonds, which significantly exceed the systematic errors for these parameters. Furthermore, the variation in bond lengths is not systematic since some bonds are shortened in **2A** with respect to **2B** and vice versa. These uncorrelated changes in bond lengths lead to different degrees of distortion for the coordination polyhedra, which can compensate each other. The observed variations in bond lengths cannot be rationalized in terms of the H-bond strengths since the distance between the proton and the acceptor atom for the same pairs of atoms coincides within 0.01 Å, so that stacking interactions have to be considered in more detail.

In the crystal of **2**, there are four independent phen ligands, and only two of them, N(1B)÷N(10B) and N(1C)÷N(10C), belonging to **2A** and **2B**, participate in rather strong $\pi$-stacking interactions. These interactions assemble molecules into dimers (see Figure 2a) with a pronounced overlap area and C···C contacts as short as 3.2−3.3Å. The dimers are interconnected in chains by other $\pi$-stacking interactions having a smaller overlap area but also displaying short interplanar distances (ca. 3.2 Å, see Figure 2b) and a parallel arrangement of phen rings (∼6°). The remaining phen ligands (N(1A)÷N(10A) and N(1D)÷N(10D)) also formally participate in stacking interactions, but ring planes are not parallel (20°), and only one shortened C···C contact is observed (3.39 Å). Interestingly, maximum differences in Eu−N distances (0.045(3) and 0.024(3)Å) are observed for ligands involved in stacking interactions, while these differences are significantly smaller (0.006−0.008(3)Å) for all others.

A similar influence of stacking interactions on Eu−N distances is found for **1Eu** and **3** (Figures S1 and S2, Supporting Information). In **1Eu**, the most pronounced stacking interaction is observed between the two phen ligands (interplanar distance 3.4 Å), which are symmetrically dependent, causing an elongation of the Eu−N bond length by 0.025(2) Å for the N(1) atom involved in this interaction. On the other hand, the Eu−N distances are almost equal for the other phen ligand (N(1′)÷N(10′)), which is only partially involved in $\pi$-stacking interactions; it is noteworthy that a rather unusual Cl···$\pi$ interaction with a Cl(3)···C(2′) contact equal to 3.569(2)Å is observed.[27] In **3**, $\pi$-stacking interactions are similar to those of the second type observed for **2**: a

(26) Chatterjee, A.; Maslen, E. N.; Watson, K. J. *Acta Crystallogr., Sect. B* **1988**, *44*, 381–386.
(27) Mooibroek, T. J.; Black, C. A.; Gamez, P.; Reedijk, J. *Cryst. Growth Des.* **2008**, *8*, 1082–1093.

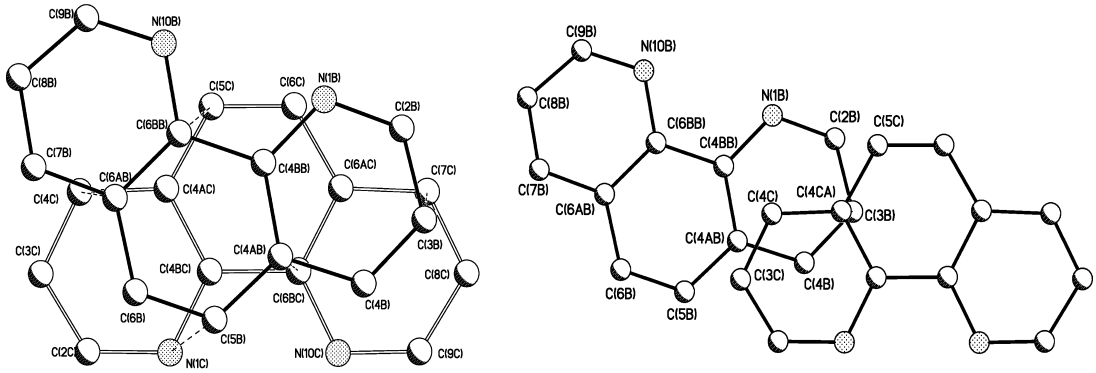


**Figure 2.** Two types of stacking interactions in the crystal of **2** between two independent molecules.

small overlap area and a shortest C···C contact equal to 3.267(4)Å prevail for the two aromatic rings containing N(10), resulting in an elongation of the Eu(1)−N(10) distance compared to Eu(1)−N(1).

A noteworthy outcome of the above description is that noncovalent interactions can alter the bond lengths in the coordination polyhedron. The reverse situation, that is, variation in H-bond strength and stacking geometry upon shrinking the coordination sphere due to lanthanide contraction, is evidenced in the isostructural series **1Eu**, **1Gd**, and **1Tb**. It was shown recently that lanthanide contraction in different isostructural series generates various effects depending on the rigidity of the ligands and crystal packing effects.[28] A comparison between **1Eu**, **1Gd**, and **1Tb** reveals that the Ln−ligand bond lengths decrease by 0.021−0.027(1)Å for Ln−O and Ln−N bonds and by 0.015(1)Å for Ln−Cl (Table S5, Supporting Information), similarly to what was reported previously, for instance, for a series of 10 isomorphous lanthanide complexes of a chiral macrocyclic ligand.[29] On the other hand, the maximum difference in the average donor−acceptor distance between **1Eu** and **1Tb** amounts to 0.004(1) Å only, with a maximum value of 0.014 Å for the O(2)−H(2OA)···Cl(1) bond (Table S6, Supporting Information). It is noteworthy that the latter H bond is the only one in **1Eu**, **1Gd**, or **1Tb** formed by atoms simultaneously coordinated to the metal ion. The stacking interactions are also independent from the lanthanide ion, within experimental error. These findings are in line with available literature data, for example, for the isostructural series $[Ln(H_2O)_9](SO_3CF_3)_3$.[26] At the same time, other specific interactions become more sensitive to lanthanide contraction. For example, the Cl···C distance of the Cl···$\pi$ interaction varies in the range 3.555−3.569 Å. Therefore, the effect of the lanthanide contraction on the chloride anion is approximately twice less compared to oxygen and nitrogen atoms.

**3.2. Charge Density Analysis.** In order to obtain direct information on the relative energy of Ln···ligand bonds and specific noncovalent interactions in the crystals, we have performed a charge density analysis according to Bader's "Atoms in Molecule" (AIM) theory[30] on the **1Gd** crystal, which was of excellent diffraction quality.

Topological analysis of the electron density distribution function $\rho(\mathbf{r})$ derived from experimental data and ab initio calculations in conjunction with Espinosa's correlation scheme[31] makes possible the estimate of the interaction energy ($E_{cont}$) with sufficient accuracy.[10,32] The good agreement between the sublimation enthalpy for molecular crystals obtained by the summation of $E_{cont}$ and thermochemical data[32] justifies this approach. The latter is not only valid for weak interactions such as H···H and C−H···O contacts (i.e., so-called closed-shell interactions [33]) but also for Mg···C and Ca···C (ca. 10−12 kcal/mol)[34] and moderate and strong H bonds (ca. 20−30 kcal/mol)[32e,35] corresponding to an intermediate type of interatomic interactions in some limiting cases (see for instance refs 32e and 35 and references therein). Assuming that Ln−X bonds correspond to at least

(28) Seitz, M.; Oliver, A. G.; Raymond, K. N. *J. Am. Chem. Soc.* **2007**, *129*, 11153–11160.
(29) Parker, D.; Puschmann, H.; Batsanov, A. S.; Senanayake, K. *Inorg. Chem.* **2003**, *42*, 8646–8651.
(30) Bader, R. F. W. *Atoms In Molecules. A Quantum Theory*; Clarendron Press: Oxford, 1990; p 395.
(31) (a) Espinosa, E.; Molins, E.; Lecomte, C. *Chem. Phys. Lett.* **1998**, *285*, 170–173. (b) Espinosa, E.; Alkorta, I.; Rozas, I.; Elguero, J.; Molins, E. *Chem. Phys. Lett.* **2001**, *336*, 457–461.
(32) (a) Lyssenko, K. A.; Nelyubina, Yu. V.; Kostyanovsky, R. G.; Antipin, M. Yu. *ChemPhysChem* **2006**, *7*, 2453–2455. (b) Lyssenko, K. A.; Korlyukov, A. A.; Golovanov, D. G.; Ketkov, S. Y.; Antipin, M. Yu. *J. Phys. Chem. A* **2006**, *110*, 6545–6551. (c) Lyssenko, K. A.; Korlyukov, A. A.; Antipin, M. Yu. *Mendeleev Commun.* **2005**, 90–92. (d) Glukhov, I. V.; Lyssenko, K. A.; Korlyukov, A. A.; Antipin, M. Yu. *Faraday Discussions* **2007**, *135*, 203–215. (e) Lyssenko, K. A.; Antipin, M. Yu. *Russ. Chem. Bull.* **2006**, *55*, 1–15.
(33) According to the AIM theory, interatomic interactions fall into "shared" and "closed-shell" types (Bader, R. F. W.; Essén, H. *J. Chem. Phys.* **1984**, *80*, 1943–1960. ). Shared interactions are characterized by negative $\nabla^2\rho(\mathbf{r})$ values and high $\rho(\mathbf{r})$ values in CP (3,−1), while in the case of closed-shell interactions (ionic bonds, some van der Waals complexes, etc.), the value of $\nabla^2\rho(\mathbf{r})$ is positive and the total $\rho(\mathbf{r})$ in CP (3,−1) is small. However, a positive $\nabla^2\rho(\mathbf{r})$ value is not a unique criterion of the closed-shell interaction. The necessary condition for realization of this type of interaction is a positive value of the energy density which is related to $\nabla^2\rho(\mathbf{r})$ by equation $h_e(\mathbf{r}) = v(\mathbf{r}) + g(\mathbf{r}) = g(\mathbf{r}) - 1/4\nabla^2\rho(\mathbf{r})$, where $v(\mathbf{r})$ and $g(\mathbf{r})$ are potential and kinetic energy densities, respectively. The value of $h_e(\mathbf{r})$ may still remain negative if the potential energy density (*a priori* negative) exceeds the kinetic one in absolute value. Therefore, the bonds which are characterized by a positive value of $\nabla^2\rho(\mathbf{r})$ and negative value of $h_e(\mathbf{r})$ are referred to as an intermediate type of interatomic interaction.
(34) (a) Pidko, E. A.; Xu, J.; Mojet, B. L.; Lefferts, L.; Subbotina, I. R.; Kazansky, V. B.; van Santen, R. A. *J. Phys. Chem. B* **2006**, *110*, 22618. (b) Pidko, E. A.; van Santen, R. A. *ChemPhysChem* **2006**, *7*, 1657.
(35) Sobczyk, L.; Grabowski, S. J.; Krygowski, T. M. *Chem. Rev.* **2005**, *105*, 3513.

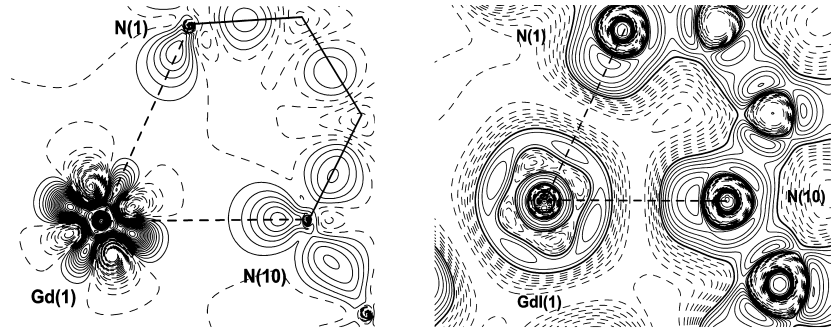


**Figure 3.** Section of DED (A) and ELF (B) in the plane of Gd(1), N(1), and N(10) atoms in **1Gd**. The ELF and DED contours are drawn with 0.05 $e$ Å$^{-3}$ steps; the values of ELF below 0.5 and negative values of DED hereafter are dashed; the value of ELF equal to 0.5 is marked in bold.

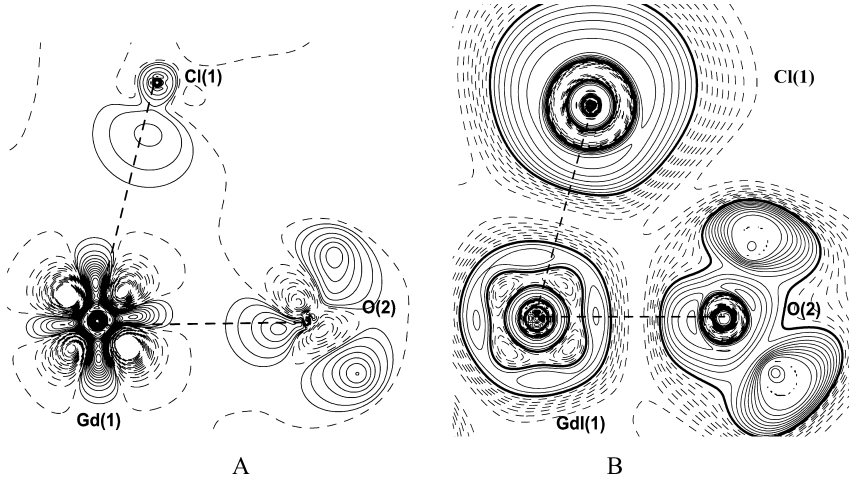


**Figure 4.** Section of DED (A) and ELF (B) in the plane of Gd(1), O(2), and Cl(1) atoms in **1Gd**. The ELF and DED contours are drawn with 0.05 $e$ Å$^{-3}$ increments.

an intermediate type of interactions, Espinosa's correlation to energy estimation in **1Gd** has been used. Although a number of investigations of charge density have appeared for compounds containing heavy atoms,[11,36] a topological analysis of $\rho(\mathbf{r})$ in crystals and isolated complexes of 4f metals has not yet been performed, to the best of our knowledge. The available experimental investigations on this topic are limited to an analysis of dynamic deformation electron density (DED) in the isostructural series of $[Ln(H_2O)_9][CF_3SO_3]_3$[37] and to the estimation of atomic charges with a charge density analysis of a $Y^{III}$ semiquinonato complex.[38] Theoretical works on this topic are limited to (i) the analysis of DED for some lanthanide complexes such as $[Ln(H_2O)_9]^{3+}$, $[Ln(DPA)_3]^{-3}$, and $[Ln(DOTAM]^{3+}$ (where DPA = pyridine-2,6-dicarboxylate; DOTAM = 1,4,7,1-tetracarbamoylmethyl-1,4,7,10-tetraazacyclododecane; Ln = Y, La, Lu),[39] (ii) the estimation of metal charges within AIM in $F_3NdCO$, and (iii) qualitative inspection of Laplacian maps in Gd complexes with DOTA and DTPA.[40] Therefore, direct estimations of covalent bonding contributions for chemical bonds formed by lanthanide ions are not available, so conclusions reached about covalent contributions in lanthanide−ligand bonds and based on the presence of electron domains in the DED distribution in the vicinity of the lanthanide (which were interpreted as arising from f electrons)[37,39] are debatable. For instance, maxima in DED can also be the consequence of some artifact (due to the use of a promolecule as the reference function).[41] Thus, in addition to DED, the more theoretically sound electron localization function (ELF) has to be used,[42] and we have calculated it from the experimental X-ray diffraction (XRD) data with Tsirelson's approach.[43] The applicability of this method for localizing domains corresponding to metal orbitals and electron lone pairs was indeed demonstrated in a number of investigations.[32b,44]

The main features of the electronic density around $Gd^{III}$ obtained from both DED and ELF are rather similar (Figures 3 and 4), and the presence of four maxima allows one to assign them to 4f electrons. The lone pairs of all N, O, and

(36) Cortés-Guzmán, F.; Bader, R. F. W. *Coord. Chem. Rev.* **2005**, *249*, 633–662.
(37) Chatterjee, A.; Maslen, E. N.; Watson, K. J. *Acta Crystallogr., Sect. B* **1988**, *44*, 386–395.
(38) Claiser, N.; Souhassou, M.; Lecomte, C.; Gillon, B.; Carbonera, C.; Caneschi, A.; Dei, A.; Gatteschi, D.; Bencini, A.; Pontillon, Y.; Lelièvre-Berna, E. *J. Phys. Chem. B* **2005**, *109*, 2723–2732.
(39) Furer, E.; Costuas, K.; Rabiller, P.; Maury, O. *J. Am. Chem. Soc.* **2008**, *130*, 2180–2183.
(40) Hess, B. A.; Kędziorski, A., Jr.; Smentek, L.; Bornhop, D. J. *J. Phys. Chem. A* **2008**, *112*, 2397–2407.
(41) Lysenko, K. A.; Antipin, M. Yu.; Khrustalev, V. N. *Russ. Chem. Bull.* **2001**, *50*, 1539–1549.
(42) Savin, A.; Nesper, R.; Wengert, S.; Fassler, T. *Angew. Chem., Int. Ed. Engl.* **1997**, *36*, 1809–1832.
(43) Tsirelson, V.; Stash, A. *Chem. Phys. Lett.* **2002**, *351*, 142–148.
(44) (a) Lyssenko, K. A.; Grintselev-Knyazev, G. V.; Antipin, M. Y. *Mendeleev Commun.* **2002**, 128–130. (b) Lyssenko, K. A.; Antipin, M. Yu.; Gurskii, M. E.; Bubnov, Yu. N.; Karionova, A. L.; Boese, R. *Chem. Phys. Lett.* **2004**, *384*, 40–44.

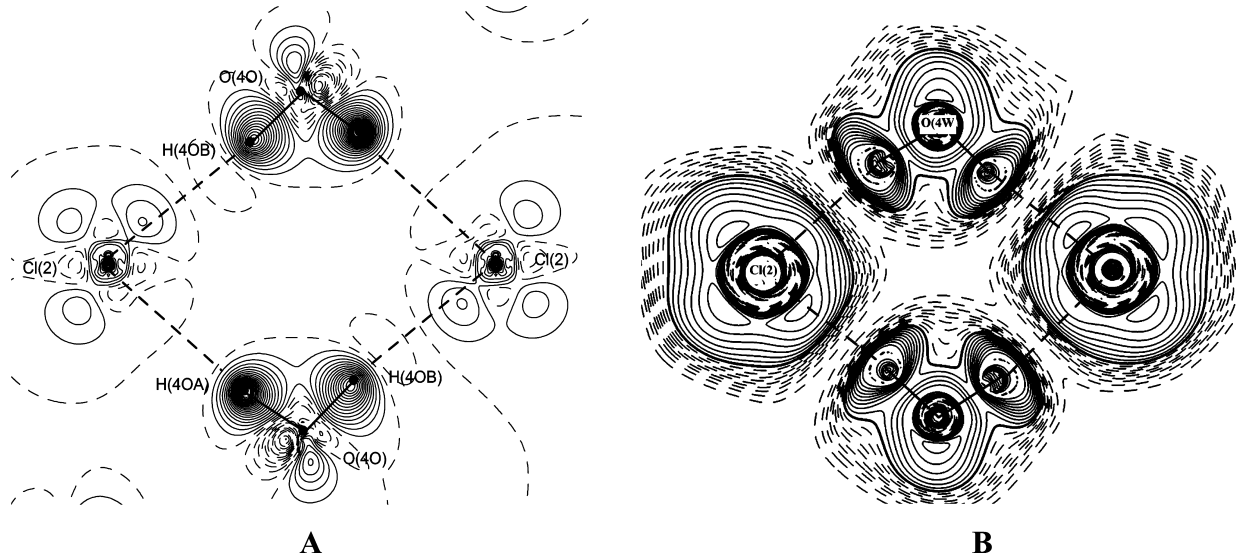


**Figure 5.** The DED (A) and ELF (B) map for the four-membered H-bonded $(Cl-H_2O)_2$ cycle in **1Gd**. The ELF and DED contours are drawn with 0.05 $e$ Å$^{-3}$ increments.

**Table 3.** Topological Parameters in the Critical Points (3,−1) for Interactions Formed by Gadolinium Atoms in **1Gd**[a]

| bond | $\rho(\mathbf{r})/e$ Å$^{-3}$ | $\nabla^2\rho(\mathbf{r})/e$ Å$^{-5}$ | $V(\mathbf{r})$/au | $h_e(\mathbf{r})$/au | ellipticity | $d_1$/Å | $d_2$/Å | $E_{cont}$/kcal·mol$^{-1}$ |
|---|---|---|---|---|---|---|---|---|
| Gd(1)−Cl(1) | 0.29 | 3.54 | −0.042297 | −0.0028 | 0.03 | 1.343 | 1.364 | 13.3 |
| Gd(1)−O(1) | 0.35 | 5.45 | −0.061273 | −0.00237 | 0.09 | 1.279 | 1.106 | 19.2 |
| Gd(1)−O(2) | 0.35 | 5.49 | −0.060882 | −0.00198 | 0.05 | 1.282 | 1.098 | 19.1 |
| Gd(1)−O(3) | 0.33 | 4.98 | −0.05488 | −0.00161 | 0.06 | 1.295 | 1.119 | 17.2 |
| Gd(1)−N(1) | 0.27 | 3.48 | −0.039733 | −0.00181 | 0.05 | 1.349 | 1.228 | 12.5 |
| Gd(1)−N(10) | 0.28 | 3.66 | −0.041602 | −0.00182 | 0.10 | 1.343 | 1.208 | 13.0 |
| Gd(1)−N(1′) | 0.29 | 3.52 | −0.04155 | −0.00252 | 0.05 | 1.339 | 1.224 | 13.0 |
| Gd(1)−N(10′) | 0.29 | 3.66 | −0.042496 | −0.00227 | 0.06 | 1.337 | 1.219 | 13.3 |

[a] Ellipticity is the ratio of two negative eigenvalues in BCP; $d_1$ and $d_2$ are the distances from BCP to Gd or to the corresponding atom participating in the bonding.

Cl atoms of the ligands are directed toward the above maxima around the metal. This disposition is different from the chemical bond pattern in transition metal complexes where so-called "peak-hole" types of interactions occur (see, for instance, refs 32b and 36, and references therein).

The corresponding DED and ELF maps for H bonds are characterized by the features expected for this type of specific interaction (Figure 5) and are close to the above distribution for Gd−N, Gd−O, and Gd−Cl bond; that is, the hydrogen atoms are directed toward the maxima corresponding to the lone pairs of chlorine. The DED map for the phen ligand is shown in Figure S3, Supporting Information.

Despite this similarity, the topological parameters of the H bonds and those of the corresponding bonding critical points (3,−1), or BCPs, are different from those of the Gd−X bonds. Although all bonds formed by gadolinium are characterized by positive values of $\nabla^2\rho(\mathbf{r})$, the electron energy density $h_e(\mathbf{r})$[33] at the BCPs is negative (see Table 3). Thus, according to Bader's classification,[33] all Gd−Cl, Gd−N, and Gd−O bonds correspond to intermediate types of interatomic interactions and cannot be considered as fully ionic. The covalent contribution in the Gd−ligand bonds in **1Gd** at least exceeds the corresponding one for closed-shell-type bonds of alkaline and alkaline earth metals[45] and are closer to intermediate bonds formed by transition metals in complexes.[36] In contrast, all H bonds, including the shortest ones (O−H···Cl and O−H···O), and stacking interactions between phenanthroline ligands as well as all other weak interactions, namely, C−H···O, C−H···Cl, and Cl···$\pi$ (see Table S7, Supporting Information), are characterized by positive values of both $\nabla^2\rho(\mathbf{r})$ and $h_e$(r), which is indicative of a "closed-shell interaction". Finally, C−C, C−H, C−N, C−H, and O−H bonds have negative values of $\nabla^2\rho(\mathbf{r})$ (see Table S8, Supporting Information) in the corresponding BCPs and belong to "shared interactions".

The interaction energies, $E_{cont}$, were estimated as $-0.5v(\mathbf{r})$ according to Espinosa's correlation scheme[31] and are summarized in Table 3. The largest values are observed for Gd−O bonds (17.2−19.2 kcal/mol), while the energy of the Gd−N and Gd−Cl bonds is comparable (12.5−13.3 kcal/mol). These values seem to be reasonable, at least for the Gd−O and Gd−phen bonds for which theoretical calculations are available. For instance, the energy of the Gd−$OH_2$ bond in two different isomers of $[Gd(DOTA)]^-$ calculated at the HF/6-31G* level has been found to be 17.4 and 18.1 kcal/mol.[46] Other estimates differ widely depending on the basis set and the level of calculation: 31.2 and 42.7 (B3LYP/3-21G*[47]), 28.9 and 31.2 (PM3[18]), and 6.6 and 17.8 kcal/mol (AM1/Sparkle[18]). It is noteworthy that increasing the

(45) Gibbs, G. V.; Spackman, M. A.; Jayatilaka, D.; Rosso, K. M.; Cox, D. F. *J. Phys. Chem. A* **2006**, *110*, 12259–12266.

(46) Cosentino, U.; Villa, A.; Pitea, D.; Moro, G.; Barone, V.; Maiocchi, A. *J. Am. Chem. Soc.* **2002**, *124*, 4901–4909.

(47) McNamara, J. P.; Berrigan, S. D.; Hillier, I. H. *J. Chem. Theory Comput.* **2007**, *3*, 1014–1027.

basis set leads to a significant decrease in Gd−$OH_2$ bond energy.[46] The energy of Gd−N bonds estimated in the **1Gd** crystal is comparable to the value calculated with the ADF-2004 package (GGA type of functional, TZ2P and TZP basis sets for Gd and the other atoms, respectively) for complexes of $GdF_3$ with various N-containing bi- and tridentate ligands: 28.8 kcal/mol.[48] One should stress here that the latter complexes are markedly different from **1Gd** and that the obtained experimental values for **1Gd** contain the contribution of specific solvation, which is more difficult to include in ab initio calculations.

The energies, $E_{cont}$, for H bonds obtained by the same procedure are listed in Table S7, Supporting Information. The energy of the O−H···Cl bonds is in the range 3.4−5.7 kcal/mol, O(2)−H(2OB)···Cl(2) (Cl···O = 3.058(2)Å) displaying the maximum energy. The O−H···O bond is the strongest one, with an energy of 10.9 kcal/mol, which is only marginally smaller than the energy of the Gd−Cl and Gd−N bonds and less than 2 times smaller than the energy of the Gd−$OH_2$ bond. The same tendency holds for the stacking interactions. Although each of the N···C and C···C interactions are as small as 0.8−1.2 kcal/mol, their total energy reaches 6.2 kcal/mol, almost half the energy of a Gd−N bond. The values for stacking interactions are close to available literature data for solid-state complexes[49] and isolated dimers.[50,51] On the other hand, the remaining interactions in the **1Gd** crystal have significantly smaller energies, with C−H···Cl interactions in the range 0.4−1.7 kcal/mol, while Cl···$\pi$ interactions only reach 0.9 kcal/mol, in line with values observed in ionic liquids and some chloride salts with organic cations[52] or for the Cl···$\pi$ interaction for a chloride anion encapsulated into octamethyl calyx[4]pyrrole (1.1 kcal/mol).[53]

Despite their relative weakness, the sums of the C−H···Cl and O−H···Cl interactions have approximately the same energy as the Gd−Cl bond, and as a consequence, the total interaction energy for coordinated and noncoordinated chloride anions in the crystal of **1Gd** is approximately the same: the sums of all bonding interactions for Cl(1), Cl(2), and Cl(3) ions are equal to 21.2, 19.7, and 16.9 kcal/mol, respectively. On the other hand, the same values for coordinated and noncoordinated water molecules significantly differ and are equal to 26.8−34.6 and 11.8 kcal/mol, respectively. Therefore, the two sites for chloride anions in the first and second coordination sphere are almost energetically equivalent, while coordination to the lanthanide ion is energetically preferable for water. This fact agrees with the easy replacement of chloride anions by water molecules that promotes the formation of the variety of crystal structures reported in this work.

**Table 4.** Net Charges of Gd and Bound Ligands Obtained over the Integration of Atomic Basins in the Crystal of **1Gd**

| atom /molecule | *Z*/*e* |
|---|---|
| Gd(1) | +1.50 |
| $H_2O(1)$ | −0.26 |
| $H_2O(2)$ | −0.28 |
| $H_2O(3)$ | −0.23 |
| $H_2O(4)$ (noncoord) | −0.09 |
| Phen (N(1)÷N(10)) | +0.33 |
| Phen (N(1′)÷N(10′) | +0.13 |
| Cl(1) | −0.47 |
| Cl(2) | −0.29 |
| Cl(3) | −0.33 |

The similar total energy of $E_{cont}$ for coordinated and noncoordinated chloride anions in **1Gd** should also be reflected in the atomic charges. The volumes, electronic population, and Lagrangian [$L(\mathbf{r}) = -1/4\nabla^2 \rho(\mathbf{r})$] of the $\rho(\mathbf{r})$ function were integrated over the atomic basins ($\Omega$) surrounded by a zero-flux surface (Table S9, Supporting Information). The value of the Lagrangian for every $\Omega$ should in principle be exactly zero,[30] and reasonably small numbers with an average value of $4.2 \times 10^{-5}$ au were indeed obtained. Moreover the $L(\mathbf{r})$ value for Gd(1) is also quite small ($2.1 \times 10^{-4}$ au).[54] The atomic charges estimated by integration of $\Omega$ led to a charge leakage equal to 0.01 *e*. In turn, the sum of atomic volumes in the crystal (632.51 $Å^3$) matches fairly well the volume of the independent part of the unit cell (634.735 $Å^3$), the error being only 0.3%.

It is noteworthy that the net charges of all atoms remarkably differ from their formal oxidation states (see Table 4), but they agree reasonably well with the results of Mulliken analysis for $GdX_3$ (X = F, Cl) complexes with various diimines.[55] The charge of the Gd atom is significantly lower (+1.5 *e*) than its formal value, and this charge is comparable to the one calculated with the AIM procedure for Nd, +2.07 *e* in the $NdF_3CO$ complex,[55] if one takes into account the larger electron-withdrawing effect of fluoride compared to chloride. Further comparison with published calculations is more delicate in view of the dependence of natural population analysis on the choice of the basis set.[4] The reduced charge on Gd(1) indicates the presence of charge transfers from the ligands to the metal ion. Indeed, the phen ligands are positively charged with total values equal to +0.33 and +0.13 for the two phens, N(1)÷N(10) and N(1′)÷N(10′). The net charge on the nitrogen atoms correlates with the Gd−N distance, being at a maximum (−1.12 *e*) for the longest and a minimum (−0.94 *e*) for the shortest bond. However, the difference in the total charge of the two phen ligands is likely to be connected not only with variations in the Gd−N bond length but also with the different number of weak $Cl^-$···H−C contacts, which affect the charges of the carbon and hydrogen atoms of the ligand. For instance, the N(1)÷N(10) ligand involved in the stacking interaction practically does not participate in $Cl^-$···H−C contacts, while the other ligand is involved in a number of C−H···$Cl^-$

(48) Maldivi, P.; Petit, L.; Adamo, C.; Vetere, V. *C. R. Chimie* **2007**, *10*, 888–896.
(49) Munshi, P.; Row, T. N. G. *Acta Crystallogr., Sect. B* **2006**, *62*, 612–616.
(50) Wang, W. Z.; Hobza, P. *ChemPhysChem* **2008**, *9*, 1003–1009.
(51) Meyer, E. A.; Castellano, R. K.; Diederich, F. *Angew. Chem., Int. Ed.* **2003**, *42*, 1210–1250.
(52) Wang, Y.; Li, H. R.; Han, S. J. *J. Chem. Phys.* **2006**, *124*, 044504.
(53) Gil-Ramirez, G.; Escudero-Adan, E. C.; Benet-Buchholz, J.; Ballester, P. *Angew. Chem., Int. Ed.* **2008**, *47*, 4114–4118.
(54) Grana, A. M.; Mosquera, R. A. *J. Chem. Phys.* **1999**, *110*, 6606–6616.
(55) Petit, L.; Joubert, L.; Maldivi, P.; Adamo, C. *J. Am. Chem. Soc.* **2006**, *128*, 2190–2191.

interactions (Table S7, Supporting Information) resulting in the decrease of its positive charge.

As for nitrogen atoms, the charges of the oxygen atoms correlate with the Gd−O bond length, −1.19 *e* for 2.378 Å and −1.32 *e* for 2.414 Å, indicating that the bond lengths are not only governed by electrostatics but also by a significant charge transfer from oxygen to metal. Despite this, the total charge of the water molecules is negative, with its absolute value significantly increasing upon coordination (−0.29 to −0.23 *e*) as compared to that of noncoordinated water (−0.09 *e*). This significant net charge for water molecules is the consequence of charge redistribution due to the formation of O−H···$Cl^-$ bonds. The charge transfer from chloride to the water molecules via H bonds can be proven by the significant decrease of the charge of noncoordinated chloride from −0.33 to −0.29 *e*. Assuming that the energies of cation···anion or anion···water H bonds are correlated with the degree of charge transfer,[56] we can use the experimental values of interaction energies and charges of chlorides for a semiqualitative estimation of electron density transfer from the chloride to the lanthanide. The decrease of negative charge of chlorides Cl(2) and Cl(3) by ca. 0.7 *e* costs on average 18 kcal/mol, which is the sum of all interactions formed by these ions. In turn, the interactions of Cl(1) with water and C−H hydrogen atoms (7.2 kcal/mol) will decrease its negative charge by ca. 0.3 *e*, making it possible to estimate the value of charge transfer from Cl(1) to Gd(1) as being equal to 0.23 *e*.

**3.3. Europium-Centered Luminescence.** As the europium ion is a well-known luminescence probe, giving information on the chemical surroundings and on the strength of the ligand field, luminescence data of the $Eu^{III}$ complexes **1Eu**, **2**, and **3** are analyzed in detail. Moreover, in view of the potential of the complexes described in this paper as building blocks for the assembly of new luminescent composite materials, energy migration processes are discussed in light of the structural and electron density data presented above.

The three europium complexes exhibit characteristic $Eu^{III}$ luminescence under broadband excitation at both ambient and low temperatures (Figure S4, Supporting Information). The electronic transitions $^5D_0 \rightarrow {}^7F_J$ ($J = 0, 2-6$) display the maximum possible number of Stark components, pointing to low site symmetry for the $Eu^{III}$ ions, that is, equal to or lower than $C_{2v}$. At the same time, ratios of the integrated intensities (Table S10, Supporting Information) are consistent with distortions of the idealized square antiprism coordination polyhedron evidenced by XRD data; see for instance the dihedral angle between the antiprism bases (Scheme 1, Table S1, Supporting Information) and the site symmetry of $Eu^{III}$, which is furthest from an inversion center in complex **2**.

The $^5D_0 \rightarrow {}^7F_0$ transition, for which the *J* values of both levels are 0, is usually a good indicator of the number of different metal-ion sites in a compound. According to XRD data, the crystal of **2** contains two independent molecules with the same coordination polyhedron and small differences in Eu−ligand bond lengths produced mainly by different types and strengths of stacking interactions. Interestingly, the high-resolution luminescence spectrum of this crystal at 10 K displays only one sharp and symmetrical line attributed to the $^5D_0 \rightarrow {}^7F_0$ transition with the full width at half-height (fwhh) = 0.8 $cm^{-1}$ (Figure 6). At the same time, the $^5D_0 \rightarrow {}^7F_J$ ($J = 1-2$) transitions display more than ($2J + 1$) components. We conclude that the small variations in Eu−ligand bond lengths cannot always be reflected in the shape of the $^5D_0 \rightarrow {}^7F_0$ transition,[57] possibly because variations in the nephelauxetic effects of the various donor atoms[58] cancel each other, leading to 0−0 transitions having the same energy for the two slightly different metal ion sites. A somewhat similar situation has been previously met with Schiff base complexes for which the presence of two chemical environments with a small difference in the Eu−N bond length (∼0.04 Å) caused only a slight asymmetry of the $^5D_0 \rightarrow {}^7F_0$ transition, while more than three components were observed for the $^5D_0 \rightarrow {}^7F_1$ transition.[59]

The energy of the $^5D_0$ level is different in **3** compared with that in **1Eu** and **2** ($\Delta E \approx 15$ $cm^{-1}$, Table 5). The higher energy of the $^5D_0$ level in **3** reflects a decrease in the covalent contribution, a consequence of the presence of one phen ligand in this complex instead of two in **1Eu** and **2**. The

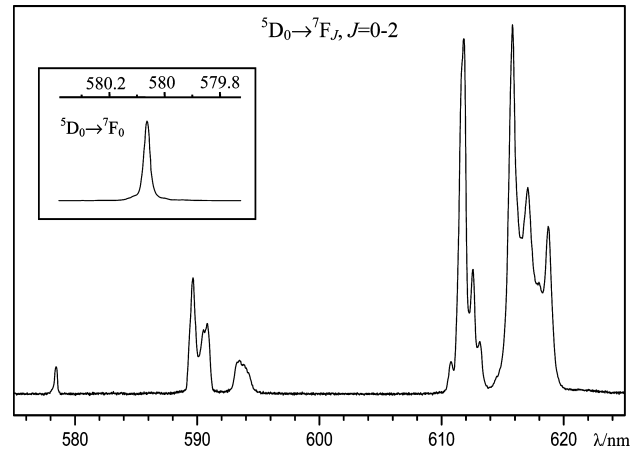


**Figure 6.** High-resolution luminescence spectrum of crystals of complex **2** at 77 K. Inset: high-resolution scan of the $^5D_0 \rightarrow {}^7F_0$ transition. Vertical scale: arbitrary units.

**Table 5.** Overall Splitting $\Delta E(^7F_J)$ of Electronic Transitions $^5D_0-{}^7F_J$ ($J = 1, 2, 4$) in the Luminescence Spectra at 77 K and Energy of the $^5D_0$ Level

| compound | $^5D_0-{}^7F_1$ | $^5D_0-{}^7F_2$ | $^5D_0-{}^7F_4$ | $E(^5D_0)$/$cm^{-1}$ |
|---|---|---|---|---|
| **1Eu** | 75[a] | 230[a] | 360[a] | 17232 |
| **2** | 110 | 175 | 350 | 17235 |
| **3** | 125[a] | 190[a] | 300[a] | 17247 |

[a] Value published in ref 15.

(56) (a) Nelyubina, Yu. V.; Antipin, M. Yu.; Lyssenko, K. A. *J. Phys. Chem. A* **2007**, *111*, 1091–1095. (b) Nelyubina, Yu. V.; Lyssenko, K. A.; Golovanov, D. G.; Antipin, M. Yu. *CrystEngComm* **2007**, *9*, 991–996. (c) Rozas, I.; Kruger, P. E. *J. Chem. Theory Comput.* **2005**, *1*, 1055–1062.

(57) It is important to note that the same crystal was used for the luminescence and X-ray diffraction experiments.

(58) Frey, S. T.; Horrocks, W. de W., Jr. *Inorg. Chim. Acta* **1995**, *229*, 383–390.

(59) Puntus, L.; Zhuravlev, K.; Lyssenko, K.; Antipin, M.; Pekareva, I. *Dalton Trans.* **2007**, 4079–4088.

energy of the $^5D_0$ level is related to the nephelauxetic effect[60] of the coordinated atoms and is described by a phenomenological equation:[58]

$$E\,(\mathrm{cm}^{-1}) = 17374 - \sum_i n_i \delta_i \qquad (1)$$

where $\delta_i$ is the nephelauxetic effect of a given donor atom and $n_i$ the number of such atoms in the inner coordination sphere; taking the accepted values for water ($-11$ cm$^{-1}$), chloride ($-22.5$ cm$^{-1}$), [58] and heterocyclic amine ($-15.3$ cm$^{-1}$),[61] the calculated value is in line with the experimental one for **2** ($\Delta E_{\mathrm{calc-exp}} = +1$ cm$^{-1}$) and **3** ($-2$ cm$^{-1}$), while it is at large variance for **1Eu** ($+25$ cm$^{-1}$). This demonstrates some limitation of the above equation: the nephelauxetic effect is very sensitive to small changes in bond distances and in the electron density on the donor atoms, and the bonding pattern analysis made for **1Gd** shows that extensive charge transfers occur.

The interaction of the lanthanide ion with the bound ligands is also reflected by vibronic satellites appearing on the electronic transitions (Figures S5−7, Supporting Information). For instance, intense satellites observed in the vibronic sideband of the $^5D_0 \rightarrow {}^7F_0$ transition in the 16 800−17 200 cm$^{-1}$ range can be assigned to $\nu$(Eu−Cl) vibrations. These vibrations have frequencies equal to 130, 140, and 127 cm$^{-1}$ for complexes **1Eu**, **2**, and **3**, respectively. The highest frequency observed for **2** reflects a stronger Eu−Cl bond, which indeed correlates with the shortest length of this bond according to XRD data. Another set of vibronic satellites is observed in the range 15 000−15 600 cm$^{-1}$; they are associated with the $^5D_0 \rightarrow {}^7F_2$ transition and have frequencies of 1418, 1420, and 1424 cm$^{-1}$ for **1Eu**, **2**, and **3**, respectively. Such a frequency corresponds to the $\nu$(C═C, C═N) vibration (see IR spectra in Figure S8, Supporting Information). The intensity of these satellites is at a maximum in **2**, which again is an indication of some transfer of charge density, usually accompanied by increasing vibronic interactions.

The splitting pattern of the electronic transitions is determined by the site symmetry of the Eu$^{III}$ ion in the crystal field and so contains the information about europium charge surroundings. Generally speaking, the overall pattern of the emission spectra is consistent with a distorted square antiprism coordination polyhedron.[62] The overall energy splitting of each transition $\Delta E(^7F_J)$ is presented in Table 5. The replacement of one chlorine anion by water molecule (comparison **1Eu/2**) increases the $\Delta E(^7F_{2,4})$ values, while $\Delta E(^7F_1)$ becomes minimum. The replacement of one phen by two water molecules (comparison **2/3**) results in an increase in $\Delta E(^7F_{1,2})$, while $\Delta E(^7F_4)$ decreases. In fact, $\Delta E(^7F_4)$ is quite similar for **1Eu** and **2** but remarkably different for **3**. Taking into account that coordinated and noncoordinated chloride anions bear charges which are not too dissimilar and that noncoordinated chlorides connect with water molecules bound to the metal ion, it is reasonable to consider the influence of second-sphere interactions. We have shown above that the latter reflect to some extent the variation in electron donation from water molecules due to an increase in O−H···Cl interactions when the distance between the metal ion and noncoordinated chloride increases. It is worth emphasizing that charge redistribution will clearly influence the net atomic charge of atoms surrounding the metal ion due to the transfer of negative charge from noncoordinated chloride anions to water molecules via H bonding. Considering the metal ion surrounding as a sphere with a radius $\approx 6$ Å (this threshold value is based on the sum of M−O bond lengths and the O···Cl separation for the H bond), we calculate that the average distances between the Eu$^{III}$ ion and noncoordinated chloride anions (NCA) amounts to 4.93, 4.87, and 4.84 Å in **1Eu**, **2**, and **3**, respectively. Taking into account these values as well as the lengths of the Eu−Cl bonds, it is logical to propose that (i) the largest $\Delta E(^7F_{2,4})$ values in **1** are probably due to both the presence of only one coordinated chloride anion that remarkably increases the asymmetry of the charge distribution in the surrounding of the Eu$^{III}$ ion, as well as the angle between strongly polarized phen ligands (Table S1, Supporting Information); (ii) the longest value for averaged NCA bonds causes the smallest $\Delta E(^7F_1)$, which is reasonable since both the first and second coordination spheres contribute to this overall splitting according to crystal field theory;[63] (iii) the smallest $\Delta E(^7F_4)$ in **3** is in line with the longest Eu−Cl$^-$ bonds (2.749(2) Å), while the largest $\Delta E(^7F_1)$ value probably arises from the strong ligand field induced by the chloride anions with the shortest averaged NCA bonds (4.84 Å).

**3.4. Energy Transfer Process.** The supramolecular network of H bonds and stacking interactions induces sizable charge redistribution within phen ligands and water molecules and affects the lanthanide chemical surroundings. As a consequence, it must also influence the ligand-to-metal energy transfer process. According to the concept of sensitized luminescence, energy absorbed by phen ligands is transferred via singlet ($^1\pi\pi^*$, 350 nm/28 570 cm$^{-1}$) and triplet ($^3\pi\pi^*$, 455 nm/22 000 cm$^{-1}$) states to the excited resonant levels of the europium ion. This is reflected in the luminescence excitation spectra, which display intense broad bands assigned to phen ligands in addition to the narrow 4f transitions (Figure 7). Interestingly, an additional weak and broad band centered at 390 nm/25 500 cm$^{-1}$ with a low-frequency edge at 450 nm/22 200 cm$^{-1}$ is observed in the excitation spectra of **1Eu** and **2**. Since a similar band is observed in the excitation spectra of **1Gd** and **1Tb** as well (Figure S9, Supporting Information), it cannot be assigned to a LMCT state. In fact, the analysis of charge density distribution performed for **1Gd** revealed that the two phen ligands bear different positive charges (0.33 and 0.13 *e*) and that the absolute charges of the nitrogen atoms are also

(60) The degree to which the term separation decreases from that of the free gaseous ion as a function of various ligand environments has been termed as the nephelauxetic effect by: Jørgensen, C. K. *Inorg. Chem.* **1962**, *4*, 73–77.

(61) Piguet, C.; Bünzli, J.-C.G.; Bernardinelli, G.; Hopfgartner, G.; Petoud, S.; Schaaad, O. *J. Am. Chem. Soc.* **1996**, *118*, 6681–6697.

(62) Lea, K. R.; Leask, M. J.; Wolf, W. P. *J. Phys. Chem. Sol.* **1962**, *23*, 1381–1405.

(63) Wybourne, B. G. *Spectroscopic Properties of Rare Earth Ions*; Interscience: New York, 1965; p 236.

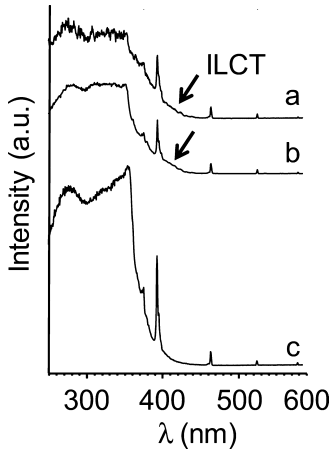


**Figure 7.** Luminescence excitation spectra at 77 K of $[EuCl_1Phen_2(H_2O)_3]Cl_2 \cdot H_2O$ (a), $[EuCl_2Phen_2(H_2O)_3]Cl_1 \cdot H_2O$ (b), and $[EuCl_2Phen(H_2O)_4]Cl_1 \cdot H_2O$ (c) at 77 K. Spectra are normalized with respect to the intensity of the magnetic dipole transition $^5D_1 \leftarrow {}^7F_0$.

different (−1.12, −1.1, −1.0, and −0.94 *e*) due to H-bonding and $\pi$-stacking interactions. Moreover the O−H···O interactions are weak in **3**. As found above, stronger and more complex $\pi$-stacking interactions in **2** compared to **1Eu**, owing to the presence of two independent molecules in the single crystal, affect the strength of the vibronic interaction and $\Delta E(^7F_J)$. In this way, it seems reasonable to assign the weak 390-nm band to an intra- or interligand charge transfer (ILCT) state caused by ligand charge redistribution. To the best of our knowledge, this is the first documented example of the influence of crystal packing on the energy transfer processes in lanthanide-containing systems. However, red-shifted luminescence from naphthalene-containing ligands due to a $\pi$-stacking interaction centered around 400 nm is known,[64] as well as the distortion of pyridine rings by intramolecular $\pi-\pi$ and CH$-\pi$ interactions in Re complexes with bipyridines, which causes a red shift in the $\pi-\pi^*$(bpy) absorption in crystalline samples.[65] There is also an example in host−guest chemistry in which the formation of strong hydrogen bonds in the outer coordination sphere of the $Eu^{III}$ ion leads to luminescence enhancement and has been used for anion recognition and analysis.[66] Therefore, the energy migration processes in the systems studied in this work can be illustrated by a simplified diagram, given in Figure 8.

The excitation spectra reported in Figure 7 are normalized to estimate the relative efficiency of the ligand excitation paths versus direct $Eu^{III}$ excitation. The highest efficiency is observed for **3**. The latter fact is comprehensible since the presence of the additional ILCT state in **1Eu** and **2** creates an extra way for the dissipation of excitation energy. This clearly demonstrates that crystal packing has a major influence on the energy transfer processes and, as a consequence, on the intensity of the $Eu^{III}$ luminescence. Moreover the presence this ILCT in the excitation spectra of terbium and gadolinium ions is quite logical since the strength and

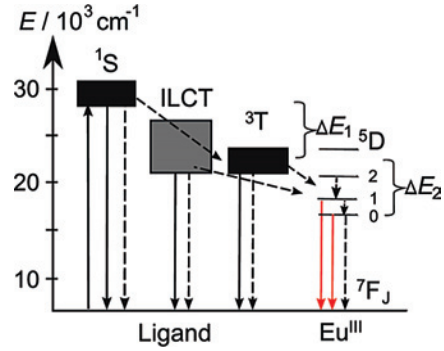


**Figure 8.** Simplified diagram of energy migration processes in considered complexes ($^1S$ = singlet state, $^3T$ = triplet state, ILCT = intraligand charge transfer state; dotted and solid lines represent nonradiative and radiative processes, respectively)

**Table 6.** Ratios $I_{tot}/I_{MD,0}$, Lifetimes, and Intrinsic $Eu^{III}$ Quantum Yields for **Eu1**, **2**, and **3** at 295 K

| | $I_{tot}/I_{MD,0}$ | $\tau_{obs}$/ms | $Q_{Eu}^{Eu} \pm 2\%$ |
|---|---|---|---|
| **1Eu** | 7.4 | 0.30 ± 0.03 | 11 |
| **2** | 9.1 | 0.38 ± 0.03 | 17 |
| **3** | 6.0 | 0.27 ± 0.02 | 8 |

type of noncovalent interactions are almost identical (see Table S6, Supporting Information) in the isostructural series of compounds **1Eu**, **1Gd**, and **1Tb**.

The efficiency of energy transfer processes in the systems studied has been estimated by the calculation of the intrinsic quantum yield of the europium-centered emission, $Q_{Eu}^{Eu}$, by means of Werts' formula.[67,68] The data reported in Table 6 correlate well with the number of innersphere water molecules, two for **2**, three for **1Eu**, and four for **3**, owing to intense dependence on nonradiative deactivation processes. The highest value of the intrinsic quantum yield is observed in **2**, which is also in line with the lowest site symmetry of the europium surroundings.

Finally, the overall absolute quantum yield $Q_{Ln}^{L}$ upon ligand excitation was measured for the most luminescent complex, **2**, and it amounts to 12.7 ± 0.3%, a substantial value taking into consideration that two water molecules are bound to the metal ion. This quantum yield is related to the intrinsic quantum yield by eq 2:

$$Q_{Ln}^{L} = \eta_{sens} \cdot Q_{Ln}^{Ln} \quad (2)$$

where $\eta_{sens}$ represents the efficacy with which electromagnetic energy is transferred from the surroundings onto the metal ion. In this case, $\eta_{sens}$ amounts to ∼0.73. This value is reasonable taking into account that energy gaps $\Delta E_1$ (6570 $cm^{-1}$) and $\Delta E_2$ (4750 $cm^{-1}$, Figure 8) are not too optimum.[69] The integrated luminescence intensity of **1Eu** and **3** was estimated relative to **2** and is equal to 0.75 and 0.43, respectively, leading to a rough estimate of $\eta_{sens}$ of 0.84 and

(64) Al-Rasbi, N. K.; Sabatini, C.; Barigelletti, F.; Ward, M. D. *Dalton Trans.* **2006**, 4769–4772.
(65) Tsubaki, H.; Tohyama, S.; Koike, K; Saitoh, H.; Ishitani, O. *Dalton Trans.* **2005**, 385–395.
(66) Gulgas, C. G.; Reinecke, T. M. *Inorg. Chem.* **2008**, *47*, 1548–1559.
(67) Werts, M. H. V.; Jukes, R. T. F.; Verhoeven, J. W. *Phys. Chem. Chem. Phys.* **2002**, *4*, 1542–1548.
(68) $Q_{Eu}^{Eu} = \tau_{obs}/\tau_R = \tau_{obs} \cdot A_{MD,0} \cdot n^3 \cdot (I_{tot}/I_{MD,0})$, where $A_{MD,0}$ is a constant spontaneous emission probability (14.65 $s^{-1}$ for $Eu^{III}$), *n* the refractive index, $I_{tot}$ the total area of the emission spectrum ($^5D_0 \rightarrow {}^7F_J$, $J$ = 0−6), and $I_{MD,0}$ the $^5D_0 \rightarrow {}^7F_1$ band area. The refractive index was taken as 1.5 for all cases.
(69) Latva, M.; Takalo, H.; Mukkala, V.-M.; Matachescu, C.; Rodríguez-Ubis, J. C.; Kankare, J. *J. Lumin.* **1997**, *75*, 149–169.

0.68 for **1Eu** and **3**, respectively. The larger $\eta_{sens}$ value obtained for **1Eu** is in line with the shortest mean lengths of the Eu−N bonds (2.566Å). The luminescence excitation spectra of **1Eu**, **2**, and **3** recorded at 295 K and normalized to the intensity of the magnetic dipole transition $^5D_1 \leftarrow {}^7F_0$ also indicate a more effective excitation of $Eu^{III}$ in **1**. The difference found between the efficiency of the energy transfer processes at low and room temperatures can be explained as follows. On one hand, the ILCT and triplet states have very similar energy in the investigated compounds (minima of the electronic state potential surfaces are around ∼22 200 and 22 000 $cm^{-1}$, respectively); on the other hand, the ILCT is typically a short-lived state,[70] while triplet states may have very long lifetimes (up to ∼1 s). Therefore, at higher temperatures, the influence of the ILCT state on the energy transfer can be considered as being negligible. Moreover, since at room temperature the population of vibronic states increases, this favors the probability of energy transfer from the singlet to triplet state, owing to the crossing of their electronic potential surfaces.

## 4. Conclusions

The detailed structural analysis of lanthanide chlorides with 1,10-phenantroline pointed out that the outersphere interactions may significantly affect the bond lengths between atoms in the inner coordination sphere. Further analysis of the peculiarities of crystal packing and bond length distribution shows that the strengths of inner and outer interactions are comparable. This proposition has been proved by the detailed analysis of the electron density distribution function in the crystal and the photophysical properties of the complexes studied. The topological analysis of electron density in **1Gd** allowed to shed a light on essential parameters of the lanthanide−ligand chemical bonds such as (i) the covalent contribution; (ii) the energy of these bonds; and (iii) the degree of ligand-to-metal charge transfer for phenanthroline, chloride, and water. This detailed analysis revealed that the energies of Ln−ligand bonds and noncovalent interactions (H bonds and $\pi$ stackings) are on the same order of magnitude. Furthermore, the presence of a network of hydrogen bonds formed by coordinated water and noncoordinated chloride anion leads to a pronounced charge transfer that is proportional to the H bonds' strength. As hydrogen bonding in the Gd complex investigated is of moderate strength, the conclusions drawn for this system can be transferred to complexes in which the counterion can potentially form H bonds, for exmple, $SO_3CF_3^-$, $MeSO_3^-$, $CF_3CO_2^-$, $Br^-$, and so on.

(70) Lewis, J. D.; Clark, I. P.; Moore, J. N. *J Phys. Chem. A* **2007**, *111*, 50–58.

The photophysical properties of the Eu complexes correlate well with their structure and with the peculiarities of chemical bonding patterns both in the inner and outer coordination spheres. In particular, the pronounced $\pi$-stacking interactions observed cause a redistribution of charges on phenanthroline ligands that leads to the appearance of an ILCT state, which to some extent participates in the sensitization of the $Eu^{III}$ luminescence. The values of the intrinsic and absolute quantum yields for metal-centered luminescence of $Eu^{III}$ indicate the relatively high efficiency of energy transfer from the surroundings onto the metal ion in the compounds considered. Additionally, the detailed analysis of the splitting pattern and overall splitting, $\Delta E(^7F_J)$, of the $Eu^{III}$ electronic transitions reveals the contribution of outersphere chloride anions to the crystal field potential owing to the transfer of negative charge to water molecules coordinated by means of H bonding.

It is worth emphasizing that the reported results represent the first attempt to shed light on the influence of crystal packing on energy transfer processes in lanthanide-containing systems by taking into account detailed structural data and experimental net atomic charges. The numerical results obtained are fully consistent, which is a good illustration that combining luminescence data with results of the detailed topological analysis of the electron density distribution function in the crystal is a good approach for a deep understanding of processes in luminescent lanthanide-containing systems. All experimental evidence accumulated in this work demonstrates the essential role of specific interionic interactions, which are usually not considered, both in theoretical works and in luminescence studies, and may considerably "perturb" the lanthanide system, changing the charge distribution around the metal ion. In such a way, it is foreseen that modulation of the weak noncovalent interactions becomes feasible by "clever crystal engineering" and therefore can be considered as a new approach for the design of luminescent materials.

**Acknowledgment.** This study was financially supported by the Russian Foundation for Basic Research (Grant nos. 06-03-32557 and 07-03-12196), the Foundation of the President of the Russian Federation (Federal Program for the Support of Young Doctors, Grants MD-172.2008.3 and MK-6026.2008.9), and Russian Science Support Foundation.

**Supporting Information Available:** Additional figures and tables and a CIF file. This material is available free of charge via the Internet at http://pubs.acs.org.

IC801402U